

Unidirectional III-V microdisk lasers heterogeneously integrated on SOI

P. Mechet,^{1,*} S. Verstyft,¹ T. de Vries,² T. Spuesens,¹ P. Regreny,³ D. Van Thourhout,¹ G. Roelkens,¹ and G. Morthier¹

¹imec - Ghent University, Photonics Research Group - Department of Information Technology (INTEC), Sint-Pietersnieuwstraat 41, 9000 Ghent, Belgium

²COBRA Research Institute, Eindhoven University of Technology, P.O. Box 512, 5600 MB, Eindhoven, The Netherlands

³Institut des Nanotechnologies de Lyon INL-UMR5270, CNRS, Université de Lyon, Ecole Centrale de Lyon, Ecully 69134, France

*Pauline.Mechet@intec.ugent.be

Abstract: We demonstrate unidirectional bistability in microdisk lasers electrically pumped and heterogeneously integrated on SOI. The lasers operate in continuous wave regime at room temperature and are single mode. Integrating a passive distributed Bragg reflector (DBR) on the waveguide to which the microdisk is coupled feeds laser emission back into the laser cavity. This introduces an extra unidirectional gain and results in unidirectional emission of the laser, as demonstrated in simulations as well as in experiment.

© 2013 Optical Society of America

OCIS codes: (140.3460) Lasers; (130.0130) Integrated optics; (130.3120) Integrated optics devices; (230.0230) Optical devices; (230.1150) All-optical devices.

References and links

1. M. Sorel, P. J. R. Laybourn, G. Giuliani, and S. Donati, "Unidirectional bistability in semiconductor waveguide ring lasers," *Appl. Phys. Lett.* **80**(17), 3051–3053 (2002).
2. M. T. Hill, H. J. S. Dorren, T. De Vries, X. J. M. Leijtens, J. H. Den Besten, B. Smalbrugge, Y. S. Oei, H. Binsma, G. D. Khoe, and M. K. Smit, "A fast low-power optical memory based on coupled micro-ring lasers," *Nature* **432**(7014), 206–209 (2004).
3. L. Liu, R. Kumar, K. Huybrechts, T. Spuesens, G. Roelkens, E.-J. Geluk, T. de Vries, P. Regreny, D. Van Thourhout, R. Baets, and G. Morthier, "An ultra-small, low-power, all-optical flip-flop memory on a silicon chip," *Nat. Photonics* **4**(3), 182–187 (2010).
4. D. Liang, M. Fiorentino, T. Okumura, H.-H. Chang, D. T. Spencer, Y.-H. Kuo, A. W. Fang, D. Dai, R. G. Beausoleil, and J. E. Bowers, "Electrically-pumped compact hybrid silicon microring lasers for optical interconnects," *Opt. Express* **17**(22), 20355–20364 (2009).
5. A. W. Fang, R. Jones, H. Park, O. Cohen, O. Raday, M. J. Paniccia, and J. E. Bowers, "Integrated AlGaInAs-silicon evanescent race track laser and photodetector," *Opt. Express* **15**(5), 2315–2322 (2007).
6. J. P. Hohimer, G. A. Vawter, and D. C. Craft, "Unidirectional operation in a semiconductor ring diode laser," *Appl. Phys. Lett.* **62**(11), 1185–1187 (1993).
7. A. W. Fang, R. Jones, H. Park, O. Cohen, O. Raday, M. J. Paniccia, and J. E. Bowers, "Integrated AlGaInAs-silicon evanescent race track laser and photodetector," *Opt. Express* **15**(5), 2315–2322 (2007).
8. C. J. Born, S. Yu, M. Sorel, and P. J. R. Laybourn, "Controllable and stable mode selection in a semiconductor ring laser by injection locking," in *Proceedings of the Conference on Lasers and Electro-Optics CLEO '03*, (Baltimore, Maryland, 2003), pp. 1–3, paper CWK4.
9. A. F. J. Levi, R. E. Slusher, S. L. McCall, J. L. Glass, S. J. Pearton, and R. A. Logan, "Directional light coupling from microdisk lasers," *Appl. Phys. Lett.* **62**(6), 561–564 (1993).
10. J. U. Nöckel, A. D. Stone, and R. K. Chang, "Q spoiling and directionality in deformed ring cavities," *Opt. Lett.* **19**(21), 1693–1695 (1994).
11. Q. J. Wang, C. Yan, N. Yu, J. Unterhinninghofen, J. Wiersig, C. Pflügl, L. Diehl, T. Edamura, M. Yamanishi, H. Kan, and F. Capasso, "Whispering-gallery mode resonators for highly unidirectional laser action," *Proc. Natl. Acad. Sci. U.S.A.* **107**(52), 22407–22412 (2010).
12. D. Liang, S. Srinivasan, D. A. Fattal, M. Fiorentino, Z. Huang, D. T. Spencer, J. E. Bowers, and R. G. Beausoleil, "Teardrop reflector-assisted unidirectional hybrid silicon microring lasers," *IEEE Photon. Technol. Lett.* **24**(22), 1988–1990 (2012).

13. F. Van Laere, G. Roelkens, M. Ayre, J. Schrauwen, D. Taillaert, D. Van Thourhout, T. F. Krauss, and R. Baets, "Compact and highly efficient grating couplers between optical fiber and nanophotonic waveguides," *J. Lightwave Technol.* **25**(1), 151–156 (2007).
14. M. Sorel, G. Giuliani, A. Scire, R. Miglierina, S. Donati, and P. J. R. Laybourn, "Operating regimes of GaAs-AlGaAs semiconductor ring lasers: experiment and model," *IEEE J. Sel. Top. Quantum Electron.* **39**(10), 1187–1195 (2003).
15. T. Numai, "Analysis of signal voltage in a semiconductor ring laser gyro," *IEEE J. Sel. Top. Quantum Electron.* **36**(10), 1161–1167 (2000).
16. E. J. D'Angelo, E. Izaguirre, G. B. Mindlin, G. Huyet, L. Gil, and J. R. Tredicce, "Spatiotemporal dynamics of lasers in the presence of an imperfect O(2) symmetry," *Phys. Rev. Lett.* **68**(25), 3702–3705 (1992).
17. M. Sargent 3rd, "Theory of a multimode quasiequilibrium semiconductor-laser," *Phys. Rev. A* **48**(1), 717–726 (1993).
18. J. Van Campenhout, "Thin-Film microlasers for the integration of electronic and photonic integrated circuits," PhD thesis, Ghent University (2007).
19. M. Sorel, P. J. R. Laybourn, A. Scirè, S. Balle, G. Giuliani, R. Miglierina, and S. Donati, "Alternate oscillations in semiconductor ring lasers," *Opt. Lett.* **27**(22), 1992–1994 (2002).
20. T. Spuesens, F. Mandorlo, P. Rojo-Romeo, P. Regreny, N. Olivier, J.-M. Fedeli, and D. Van Thourhout, "Compact integration of optical sources and detectors on SOI for optical interconnects fabricated in a 200mm CMOS pilot line," *J. Lightwave Technol.* **30**(11), 1764–1770 (2012).

1. Introduction

Directional bistability, i.e. the ability of a laser to operate either in the clock-wise (CW) or counter-clock-wise (CCW) mode, is a unique characteristic of ring and disk lasers [1]. The bistability of microring lasers was used to demonstrate optical switching and logic applications [2,3]. This feature has also been observed in racetrack ring lasers and microring lasers built on a hybrid silicon platform [4,5]. Bistability is useful for some applications, but is undesirable for microdisk lasers used in optical interconnects. Indeed, different devices belonging to the same design can lase in different directions or switch from one lasing direction to the other depending on the injection current and the temperature. Stable unidirectional lasing ensures a higher efficiency of the laser and has been demonstrated using several approaches. "S-shape" ring resonator cavities are designed to introduce asymmetric coupling between the CW and the CCW modes [6]. In order to increase the net modal gain in one direction, the injection of an optical pulse from an external laser or light emitting diode (LED) has also been used [1,7,8]. These approaches require an external light source or introduce additional optical loss, which either degrades the laser performance or increases the complexity of the total system and its power consumption. Another approach is to break the rotational symmetry by using deformed optical microcavities to increase the directionality of emission and power collection efficiency [9]. However, all deformed cavities have the problem that the quality factor (Q factor) significantly decreases as the deformation increases [10]. Highly unidirectional laser action from whispering-gallery modes has been demonstrated with an elliptical-shape quantum cascade laser microcavity with a wavelength-size notch at the boundary [11].

Another approach is to rely on an integrated optical reflector, such as a teardrop reflector, at one end of the bus waveguide. The reflector induces the laser to emit light toward the other end. Compared with external injection from another laser, this approach does not require additional power consumption or additional complexity and is free of mismatch in wavelength between the two lasers. Unidirectional operation of a hybrid silicon microring laser coupled to a waveguide with such a teardrop reflector is investigated in [12]. However, the hybrid microring laser in that work had a diameter of 50 μm , and was operated at 30mA bias current. Under these experimental conditions, unidirectionality was qualitatively demonstrated although the laser does not necessarily operate in single-mode operation. In this paper we demonstrate unidirectional lasing of single-mode hybrid silicon microdisk lasers operating in continuous-wave at room temperature. We provide quantitative experimental results as well as a numerical analysis. The devices have a diameter of 7.5 μm and are electrically pumped. Extra power consumption and added complexity to the design are not

necessary to achieve unidirectionality as the system relies on a distributed Bragg reflector integrated in the silicon-on-insulator (SOI) circuit.

2. Device design and integration technology

We fabricated the unidirectional microdisk laser shown schematically in Fig. 1. A microdisk is etched into an InP-based film that is bonded onto a patterned SOI waveguide structure. The InP etch is not complete so that an electrical bottom contact can be defined. The disk edge is laterally aligned to an underlying SOI wire waveguide (WG).

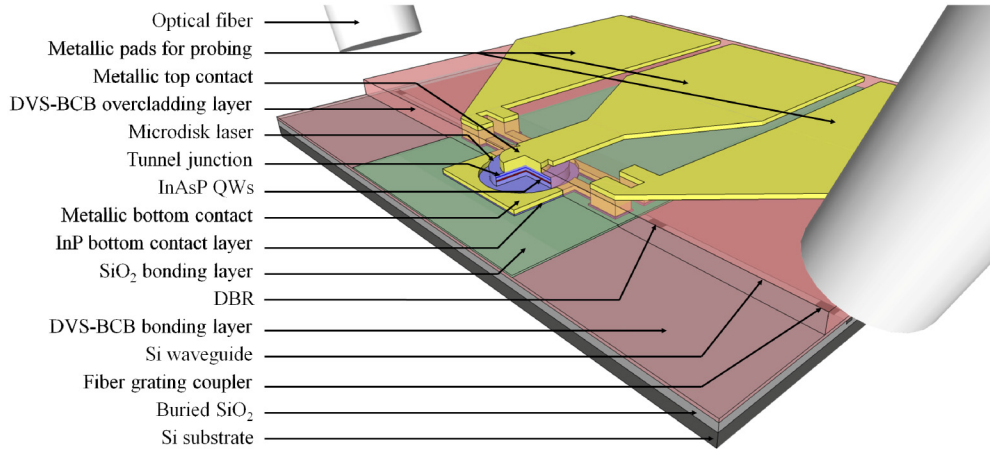


Fig. 1. Schematic view of an InP-based microdisk laser heterogeneously integrated on SOI. The laser emission under electrical pumping of the microdisk evanescently couples to an underlying Si WG. The light is coupled out of the chip using grating couplers, and is collected with optical fibers. A DBR structure can be found on one side of the WG.

Two optical levels can be identified in Fig. 1. The lowest level consists of narrow single mode SOI waveguides embedded in SiO_2 (with a width of 600nm and a height of 220nm). The upper level consists of a 583nm thick InP-based membrane. The microdisk lasers consist of a 483 nm thin disk cavity on top of a 100 nm thin InP bottom contact layer. The active layers consist of three compressively strained InAsP quantum wells (QWs) emitting around 1530nm and are surrounded by an n-doped layer on the bottom and a p-doped layer on the top to form the diode structure. A tunnel junction is implemented on the p-side such that an n-type contact layer can be used instead of a heavily doped p-type contact layer, in order to significantly reduce optical absorption. The tunnel junction also ensures uniform current injection over the disk. The two levels are separated by a thin transparent layer (50nm) of a low refractive index material ($n = 1.54$ for divinylsiloxane-bis-benzocyclobutene (DVS-BCB)) and 65nm of SiO_2 ($n = 1.47$), allowing evanescent coupling to the underlying waveguide. The designed microdisk lasers have a diameter of 7.5 μm . A distributed Bragg reflector (DBR) implemented at one end of the bus waveguide forces the laser to emit light towards the other end. If the DBR structure is implemented in the CCW emission direction of the system, light emitted in the CCW mode is partially coupled back to the CW mode inside the microdisk laser. The power coupled back into the cavity leads to a photon density increase and unidirectional lasing in the desired direction. Compared with external injection from another laser this approach does not require additional power consumption and does not suffer from a potential mismatch in wavelength between the two lasers.

The SOI waveguides are fabricated in a CMOS fab using 193nm deep ultra-violet (DUV) lithography. The design of the passive SOI circuit for the considered device consists of a 600nm-wide waveguide, tapered down on both sides to a 500nm-wide waveguide, as depicted in Fig. 2. The 500nm-wide waveguide is on one side tapered up to a 2 μm -wide waveguide,

itself tapered up to a shallow-etch (etching depth: 70nm out of the 220nm) grating coupler (GC) used to collect the laser emission from the microdisk out of the chip in a single-mode optical fiber [13]. The 500nm-wide waveguide is on the other side tapered up to a 2 μ m-wide waveguide, where the DBR structure is defined. Two DBR configurations are implemented. They are both shallow-etched and their fill-factor is 50%, but they differ in period. One of them has a period of 290nm, while the other one has a period of 300nm. The waveguide after the DBRs is in both cases further tapered to be able to define another grating coupler, used to collect the laser emission from the microdisk in a single-mode optical fiber. The fiber grating couplers are optimized to demonstrate a maximum coupling efficiency at 1.55 μ m. Above threshold, the laser emission from the microdisk is coupled to the TE mode of the waveguide, and is simultaneously collected out of both grating couplers in optical fibers under a 10 $^\circ$ angle in order to maximize the collection at 1.55 μ m. The DBR is in both cases designed to be 55 μ m away from the middle of the 600nm-wide waveguide section.

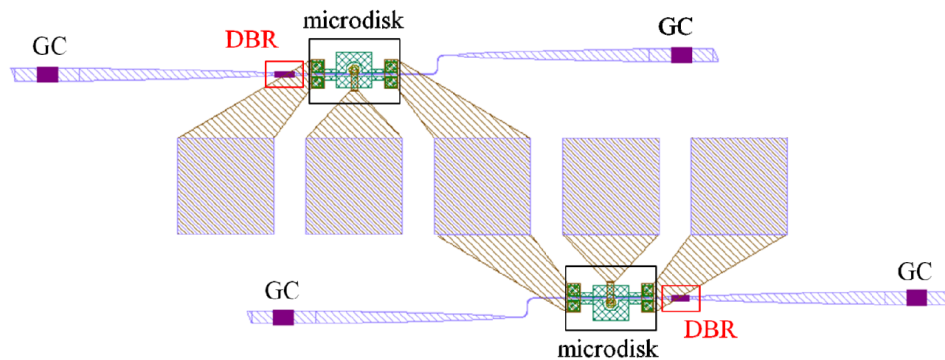


Fig. 2. Design of the fabricated microdisk lasers. The DBR structure on the top WG has a period of 300nm, while the one on the bottom WG has a period of 290nm.

The device fabrication relies on the adhesive bonding of the molecular-beam-epitaxy-grown InP-based heterostructure onto the SOI with the use of the planarizing polymer DVS-BCB. Prior to bonding, 65nm of SiO₂ is deposited on the unprocessed InP die. The III-V die is positioned upside down on top of the SOI waveguide circuit, on which DVS-BCB has been spin-coated, and the resulting bonded structure is cured. After the bonding process, the InP substrate is wet etched until only the desired epitaxial structure remains. Alignment markers for subsequent processing are defined in the Si layer relative to the waveguide structures. This allows the accurate alignment of the microdisk lasers with respect to the waveguides. A nitride hard mask is deposited by PECVD on top of the epitaxy. This layer also protects the DVS-BCB and underlying silicon waveguides in the following processing steps. The pattern is transferred into the nitride mask using Reactive Ion Etching and the microdisks are patterned in the III-V membrane using Inductively Coupled Plasma (ICP) etching. The etching is monitored in order to leave 100nm of n-doped InP as a bottom contact layer.

The next step consists in defining the metallic bottom contact with lift-off. A thin layer of Ti (40nm) is first deposited to enhance the adhesion of the metal on top of the III-V material. 50nm of Platinum and a thick gold layer (100nm) are further deposited to finish the bottom contact definition. In order to separate two adjacent microdisk lasers, the InP bottom contact layer between them is etched with ICP. The sample is then planarized by spin-coating and curing undiluted DVS-BCB. The low refractive index of this material insures good optical confinement of the laser light in the microdisk laser. It also reduces the optical losses induced by the metallic top contact as the distance between the optical mode and the metal can be made large enough. The next steps consist in opening vias in the overcladding DVS-BCB layer in order to access the metallic bottom contact and to deposit the metallic top contact with lift-off (similar recipe as for the bottom contact). Finally, a layer of gold, 800nm thick, is

deposited on the sample to define metallic pads that will be used to individually probe each microdisk laser. The thick contact also serves as a heat sink as it improves the heat dissipation under continuous-wave bias. From several cross-sections performed with Focused-Ion-Beam (FIB), we can conclude that the total bonding thickness is uniform everywhere on the sample (115nm above the waveguides). The DVS-BCB overcladding layer above the edge of the microdisk laser is 900nm thick. Figure 3 is a microscope picture of the sample where the processed microdisk lasers can be seen. The picture also illustrates the high potential for dense integration of microdisk lasers on a silicon photonic integrated circuit.

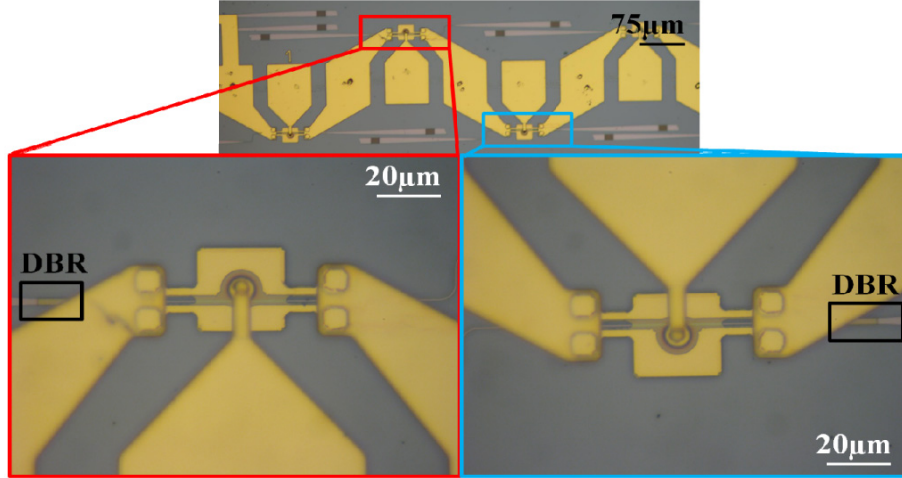


Fig. 3. Microscope pictures of the fabricated devices. The DBR structure can be seen on one side of the waveguide.

3. Simulation of the unidirectional behavior

An approximate analytical solution of the whispering gallery modes can be found by solving the Helmholtz equation in cylindrical coordinates. Because microdisk lasers do not have facets through which the light can be coupled out, an evanescent coupling towards a neighboring waveguide is assumed in this theoretical approach.

To explain the directional behavior of the microdisk lasers, we formulate the rate equations in terms of two counterpropagating whispering gallery modes with electric fields E^+ and E^- . The spontaneous emission of the microdisk laser is implemented in two electric fields $E_{noise1}(t)$ and $E_{noise2}(t)$ where $E_{noise} = RR.n.e^{2i\pi n'}$, with RR representing the spontaneous emission amplitude and n and n' random numbers between 0 and 1. We find [14,15]:

$$\frac{dE^+}{dt} = \frac{1}{2}(1-j\alpha)(G^+ - \frac{1}{\tau_p})E^+ + \frac{v_g}{2\pi R}[E_{noise1} + KE^-] \quad (3.1)$$

$$\frac{dE^-}{dt} = \frac{1}{2}(1-j\alpha)(G^- - \frac{1}{\tau_p})E^- + \frac{v_g}{2\pi R}[E_{noise2} + KE^+] \quad (3.2)$$

The model includes internal losses in the cavity through the photon-lifetime parameter τ_p . The parameter α is the linewidth enhancement factor that accounts for variations in refractive index due to carrier fluctuations in the semiconductor medium. G is the modal gain factor which will be described further and $K = K_d + jK_c$ represents an explicit linear coupling rate between the two modes where K_d is the dissipative coupling and K_c the

conservative coupling. This coupling term describes the effects of reflection at the end facets of the silicon waveguide and the coupling between the CW and the CCW modes due to sidewall roughness.

For the carrier density rate equation, we find:

$$\frac{dN}{dt} = \frac{I}{qV} - \frac{N}{\tau_c} - G^+ |E^+|^2 - G^- |E^-|^2 \quad (3.3)$$

I denotes all injected current and τ_c is the carrier lifetime. The gain experienced in a semiconductor material decreases for high optical intensity. This is due to gain suppression. Gain suppression takes place even when the total carrier density N is constant and reflects the reduction of 'resonant carriers' due to carrier heating and spectral hole burning. To account for this effect, a gain suppression is added in the denominator of the expression of the modal gain:

$$G^+ = \frac{\Gamma g_0 v_g (N - N_0)}{1 + \varepsilon_s |E^+|^2 + \varepsilon_c |E^-|^2} \quad (3.4)$$

$$G^- = \frac{\Gamma g_0 v_g (N - N_0)}{1 + \varepsilon_s |E^-|^2 + \varepsilon_c |E^+|^2} \quad (3.5)$$

where ε_s reflects the self-gain suppression and ε_c the cross-gain suppression. The confinement factor Γ is due to the limited height of the active multi-quantum well. N_0 is the transparency carrier density, g_0 is the differential gain, and v_g is the group velocity in the microdisk laser. Strain in the quantum wells has a large impact on the band structure of the active material and can have beneficial effects on the gain, by reducing the transparency carrier density and/or improving the differential gain.

The expression of the modal gain is linearized to:

$$G^+ = \Gamma g_0 v_g (N - N_0) (1 - \varepsilon_s |E^+|^2 - \varepsilon_c |E^-|^2) \quad (3.6)$$

$$G^- = \Gamma g_0 v_g (N - N_0) (1 - \varepsilon_s |E^-|^2 - \varepsilon_c |E^+|^2) \quad (3.7)$$

Calculations have shown that $\varepsilon_c = 2\varepsilon_s$ [16,17]. The cross-gain suppression ε_c will therefore break the symmetry and enforce the unidirectional operation of the laser. The gain suppression is, however, only significant when the photon density is high. This means that at lower output powers, a bidirectional regime will be present. Table 1 summarizes the parameters implemented in the numerical solving of the above set of equations. The value for the linear coupling coefficient K is chosen so that the simulation matches the experimental results.

Table 1. Values of parameters considered for the simulation of the bifurcation diagrams of the microdisk lasers.

<i>Symbol</i>	<i>Name of the parameter</i>	<i>Value</i>	<i>Unit</i>	<i>Reference</i>
τ_p	Photon lifetime	4.17	ps	[18]
τ_c	Carrier lifetime	600	ps	[18]
α	Linewidth enhancement factor	4		
v_g	Group velocity in the microdisk laser	3E8/3.4	m/s	[18]
\mathcal{E}_s	Self-gain suppression	0.1E-18	cm ⁻³	
\mathcal{E}_c	Cross-gain suppression	2 x 0.1E-18	cm ⁻³	
g_0	Differential gain	1E-16	cm ²	
N_0	Transparency carrier density	1.5E18	cm ⁻³	[18]
RR	Spontaneous emission amplitude	2		
K	Explicit normalized linear coupling rate between the two modes	$\frac{1 \cdot 10^{-4}(0.2 + j)}{ 1 + j }$		

After finding local extrema and stable solutions, the bifurcation diagram as a function of bias current is depicted in Fig. 4. We can distinguish between three different regimes. The first regime, just after threshold, is the bidirectional regime. As the optical power is low, non-linear effects can be neglected and inter-modal coupling is the dominant effect, causing the two counterpropagating modes to be equally present. When the injection current is increased, we can have a bidirectional oscillating regime. The competition between linear coupling and non-linear gain suppression results in an oscillating behavior [14,19]. In this regime, the intensities of the two counterpropagating modes are modulated with harmonic sinusoidal oscillations and share the same oscillation frequency which lies in the GHz range. The modulation is out of phase on both outputs which means that the power in one mode is high when it is low in the other mode. The graph depicts the maximal and minimal values of the mode intensities. The last regime corresponds to the unidirectional operation where the initial conditions determine which of the two modes is dominant [1]. Non-linear gain suppression is now dominant and one mode suppresses the other, resulting in unidirectional behavior. The CW mode becomes dominant in Fig. 4(a), while the CCW mode becomes dominant in Fig. 4(b), depending on the initial conditions. The noise generated by the spontaneous emission, and represented by the fields $E_{noise1}(t)$ and $E_{noise2}(t)$ in Eqs. (3.1) and (3.2), will determine if the laser lases preferentially in the CW or the CCW mode. Figure 5 illustrates the simulated bifurcation diagram of the microdisk laser, calculated with the parameters from Table 1, except that no gain suppression has been taken into account this time. Without gain suppression in the microdisk cavity, the laser will not lase unidirectionally.

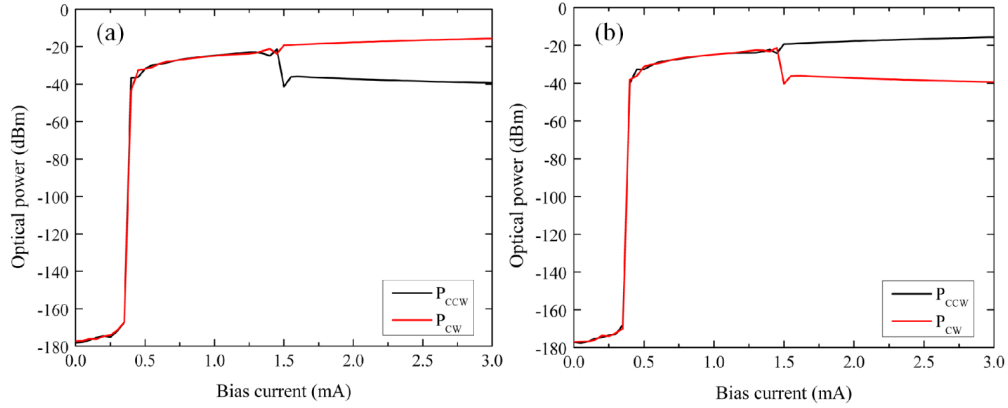


Fig. 4. Bifurcation diagrams of a 7.5 μm diameter disk. The optical power in the CW mode is plotted in red, and the optical power in the CCW mode is plotted in black. Depending on initial conditions, one of the modes becomes dominant and suppresses the other at high bias current (a) The CW mode becomes dominant, (b) The CCW mode becomes dominant).

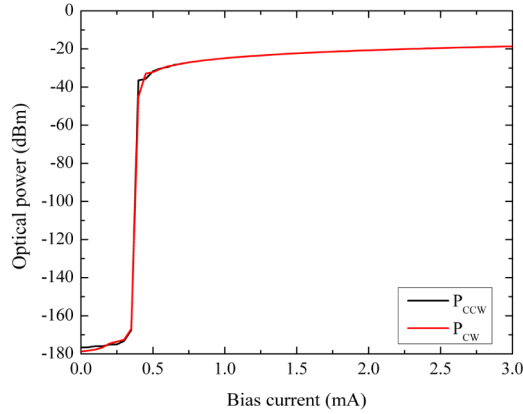


Fig. 5. Bifurcation diagrams of a 7.5 μm diameter disk: no gain suppression has been taken into account in the simulation. The optical power in the CW mode is plotted in red, and the optical power in the CCW mode is plotted in black. Unidirectional operation of the laser is not achieved without gain suppression in the microdisk cavity.

A passive optical reflector is now added to the CCW emission direction of the system, feeding laser emission propagating in the CCW direction back into the laser cavity. To simulate this effect, a new term is added to the calculation of the field propagating in the CW direction.

$$\frac{dE^+}{dt} = \frac{1}{2}(1 - j\alpha)(G^+ - \frac{1}{\tau_p})E^+ + \frac{v_g}{2\pi R}[E_{noise1} + (K + r.e^{j\Phi})E^-] \quad (3.8)$$

$$\frac{dE^-}{dt} = \frac{1}{2}(1 - j\alpha)(G^- - \frac{1}{\tau_p})E^- + \frac{v_g}{2\pi R}[E_{noise2} + KE^+] \quad (3.9)$$

The reflectivity from the bus waveguide is implemented so that the reflection induced by the DBR structure is simulated as $r.e^{j\Phi}$, where r represents the amplitude of the field reflection and Φ represents the phase of the reflected signal. Figure 6 illustrates the resulting bifurcation diagrams for different values of r and Φ . On Fig. 6(a), the phase is kept constant ($\Phi = 2\pi$) and the parameter r is swept amongst the values (0; 0.01; 0.1; 1). For $r = 0$, the

typical bifurcation diagram plotted in Fig. 4 is obtained. Even for the lowest value of r , all the optical power is coupled to the CW mode of the microdisk laser and a unidirectional regime is present. As the value of r increases, the extinction ratio of the optical power in the CW mode and the optical power in the CCW mode increases. On Fig. 6(b), the phase is kept constant ($\Phi = \frac{\pi}{2}$) and the parameter r is swept amongst the same previous values. We observe that all the optical power is also coupled to the CW mode of the microdisk laser as soon as an external reflection is added to the simulation. The extinction ratio of the optical power in the CW mode and the optical power in the CCW mode increases as a function of r .

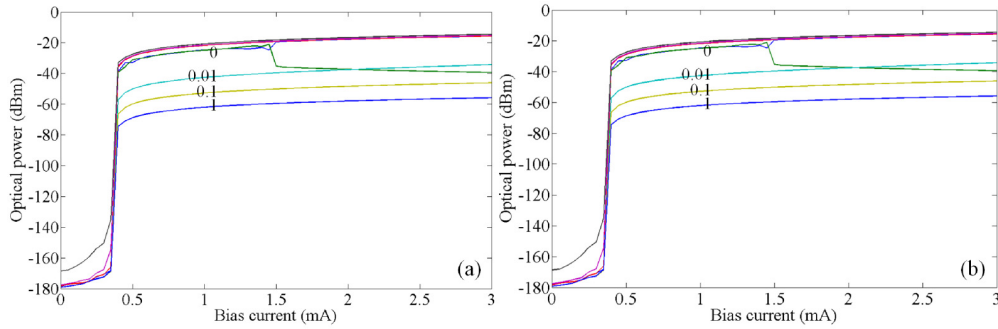


Fig. 6. Bifurcation diagrams of a 7.5 μm diameter disk coupled to a straight waveguide where a Bragg reflector is implemented on the CCW propagation direction of the system. All the power is coupled to the CW mode as soon as an external reflection is added to the system. (a) Bifurcation diagrams with a phase $\Phi = 2\pi$ for increasing values of r . (b) Bifurcation diagrams with a phase $\Phi = \frac{\pi}{2}$ for increasing values of r .

The feedback as well as the extra phase introduced by the DBR structure does not have a large impact on the threshold of the microdisk laser. This can be theoretically demonstrated by calculating the threshold gain of a microdisk laser from the coupled rate equations for the complex field amplitudes of the clockwise and counter clockwise propagating laser modes. One can demonstrate that in the static case, for which the field amplitudes (and photon numbers) are constant in time, and for bias currents close to the threshold current, where gain suppression can be neglected:

$$G_0 = \frac{1}{\tau_p} - 2\left(\frac{v_g}{2\pi R}\right)\sqrt{|K_1||K_2|}\cos\left(\frac{\Phi_1 + \Phi_2}{2}\right) \quad (3.10)$$

where τ_p is the photon lifetime, $|K_1|$ and $|K_2|$ are the amplitudes of the linear coupling coefficients K_1 and K_2 of the clockwise and the counterclockwise propagating modes respectively, and Φ_1 and Φ_2 are their phases. The photon lifetime in the simulations is 4.17ps. The first term of the threshold gain is then in the order of 10^{12} s^{-1} . On the other hand, the second term of the threshold gain is in the order of 10^9 to 10^{10} s^{-1} in case of strong back reflection, which makes its influence, including the one from the phase factor, negligible.

Simulations demonstrate that integrating a reflector on one side of the waveguide to which the microdisk is coupled feeds laser emission back into the laser cavity. This introduces an extra unidirectional gain and results in unidirectional emission of the laser.

From the above equations, we can conclude that there are two main effects in the coupling between the two modes. The cross-gain suppression prohibits the counterpropagating cavity mode to build up. This effect is necessary for unidirectional operation, but a low value of the

linear coupling K ($K = K_d + jK_c$) also favors unidirectional operation. The dissipative coupling K_d and the conservative coupling K_c describe the effects of parasitic reflection due to sidewall roughness. We can simulate the effect of the linear coupling K on the bifurcation diagram of a microdisk laser. In Fig. 7, we plot the extinction ratio in dB of the optical powers P_{CW}/P_{CCW} as a function of the ratio of $|K|$ expressed in Table 1 over the reflection from the bus waveguide r , when the microdisk is biased at 1mA. The phase Φ is kept constant while the amplitude of the field reflection r is swept.

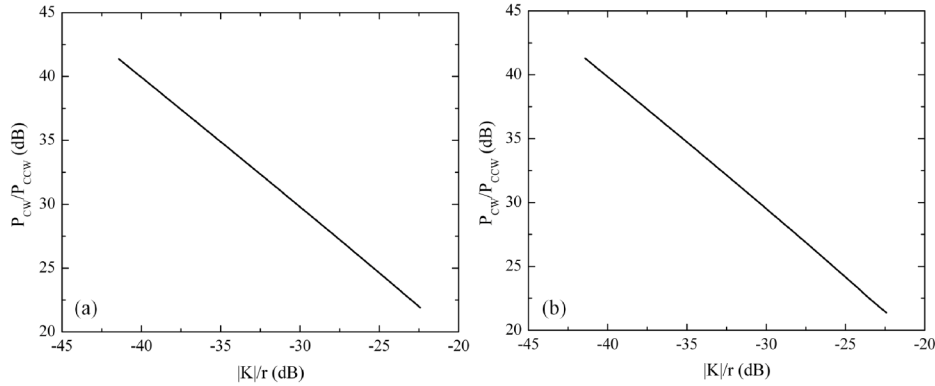


Fig. 7. Ratio of optical powers in the CW and the CCW modes as a function of the ratio of linear coupling between the modes over the amount of external reflection from the bus waveguide induced by the DBR. (a) For a phase $\Phi = 2\pi$ and values of r between 0.01 and 1.

(b) For a phase $\Phi = \frac{\pi}{2}$ for values of r between 0.01 and 1.

We demonstrate that the external reflection induced by the DBR along the CCW direction clearly influences the behavior of the microdisk laser. The linear dependence of the ratio of optical powers in dB to the ratio in dB of the linear coupling and the reflectivity indicates that the higher the external reflection from the bus waveguide, the higher the extinction ratio between the optical powers in the CW and the CCW modes. The phase of the external reflection, as well as the linear coupling K , do not have a significant impact on the slope of the linear dependence between the two ratios.

4. Experimental demonstration of the unidirectionality of microdisk lasers

The optical power-current (LI) characteristics of two $7.5\mu\text{m}$ -diameter lasers lasing in continuous-wave operation at room temperature are plotted in Fig. 8. The effective DBR length in both designs was chosen to be about $15\mu\text{m}$, with 50 periods. The microdisk laser characterized in Fig. 8(a), named Laser A, is coupled to a waveguide where a DBR with a period of 300nm is implemented in the CCW emission direction of the system. The microdisk laser characterized in Fig. 8(b), named Laser B, is coupled to a waveguide where a DBR with a period of 290nm is implemented in the CW emission direction. Thermal roll-over appears in both devices for a bias current higher than 1.5mA.

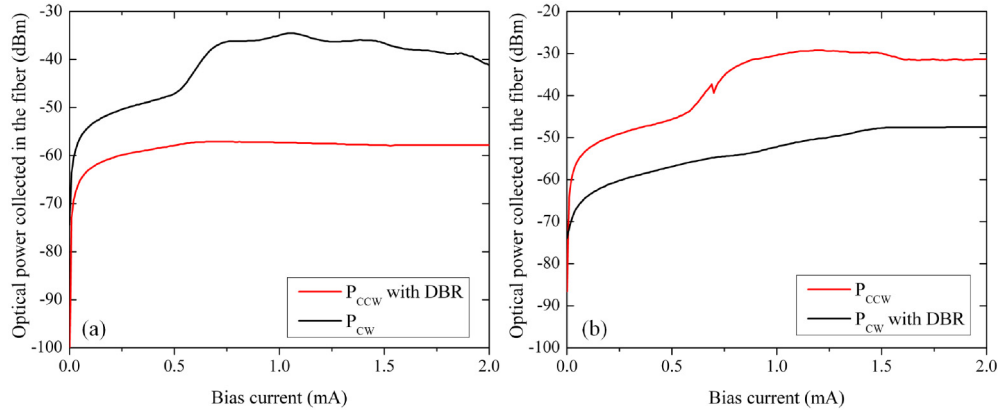


Fig. 8. LI characteristics of microdisk lasers A and B with a diameter of $7.5\mu\text{m}$. The plotted optical power is collected in optical fibers on both sides of the WGs. (a) Microdisk laser A coupled to a WG where the DBR has a period of 300nm . (b) Microdisk laser B coupled to a WG where the DBR has a period of 290nm .

The spectra of the microdisk lasers coupled to a waveguide with a DBR with a period of 300nm and a DBR with a period of 290nm are plotted in Figs. 9(a) and 9(b) respectively for 1.2mA bias (continuous wave operation at room temperature). Single-mode operation in continuous wave regime at 1554.0nm and at 1555.8nm is demonstrated for both devices respectively. A side-mode suppression ratio of 18.6dB is measured for laser A on Fig. 9(a) and is higher than 25dB for laser B on Fig. 9(b). The free-spectral range is around 27nm for both devices. At the peak lasing wavelength of the microdisk laser, the extinction ratio between the optical powers coupled out of the waveguide on the side of the DBR structure and on the side without DBR is respectively 46.1dB and 39.9dB .

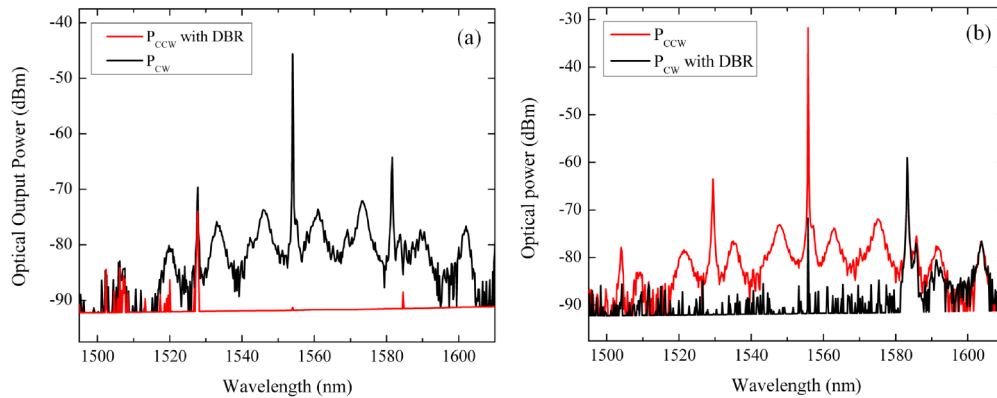


Fig. 9. Spectra of microdisk lasers A and B with a diameter of $7.5\mu\text{m}$. The plotted optical power is collected in optical fibers on both sides of the WGs. (a) Microdisk laser A coupled to a WG where the DBR has a period of 300nm . (b) Microdisk laser B coupled to a WG where the DBR has a period of 290nm .

Table 2 summarizes the wavelengths of each of the longitudinal modes, and their measured optical powers coupling out of the grating couplers on the side of the DBR and on the side without DBR.

Table 2. Spectral characteristics of microdisk lasers A and B.

Mode	Laser A			Laser B		
	λ (nm)	Optical power side w/ DBR (dBm)	Optical power side with DBR (dBm)	λ (nm)	Optical power side w/ DBR (dBm)	Optical power side with DBR (dBm)
-2				1504.0	-77.8	-88.5
-1	1527.8	-69.7	-73.9	1529.4	-63.5	-92.0
0	1554.0	-45.6	-91.7	1555.8	-31.8	-71.7
+1	1581.6	-64.2	-91.5	1583.2	-59.5	-59.0
+2	1610.2	-76.9		1612.0	-72.9	-72.4

The passive characterization of the DBR is performed on a nominally identical passive SOI design covered in DVS-BCB. Light from a tunable laser is coupled into the chip with a 10-degree angled single-mode optical fiber through a grating coupler to a waveguide where a DBR with a period of either 290nm or 300nm is present. The optical power at the output of the waveguide, i.e. after the DBR structure, is collected out of another grating coupler in a single-mode optical fiber under a 10-degree angle.

Figure 10 depicts the results of the characterization of the DBR structure with a period of 300nm [Fig. 10(a)] and with a period of 290nm [Fig. 10(b)]. In both cases, the transmission measurement is plotted together with the transmission through a straight SOI waveguide without DBR structure.

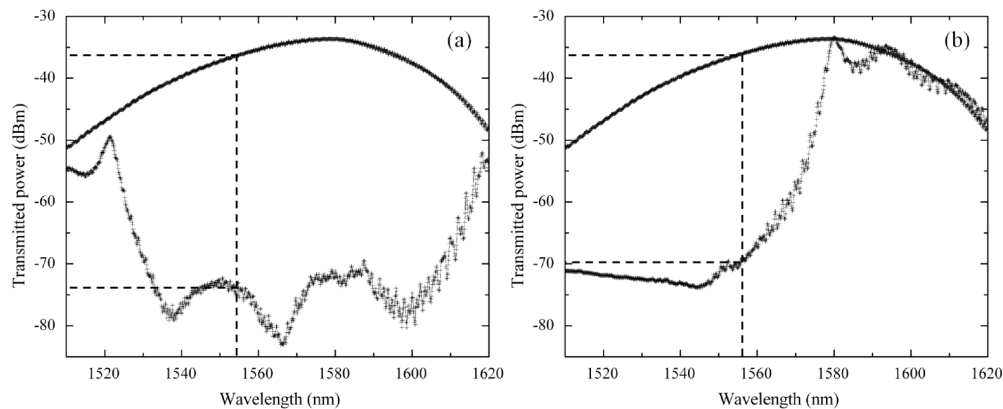


Fig. 10. Transmission characteristics of a WG where the DBR has a period of 300nm (a), and of a WG where the DBR has a period of 290nm (b). The transmission characteristic of a straight WG of the same sample, acting as reference, is systematically plotted.

The peak efficiency of the grating couplers on this sample is located at 1580.5nm due to the BCB top cladding layer. On Fig. 10(a), an extinction ratio at the peak lasing wavelength of the microdisk laser (1554.0nm) of 38.1dB is measured between the reference transmission and the transmission through the DBR structure. In the case of Fig. 10(b), an extinction ratio at the peak lasing wavelength of the microdisk laser (1555.8nm) of 33.1dB is measured. Even though the reflection induced by the DBR structure is close to 100%, the low coupling efficiency between the microdisk laser and the silicon waveguide lowers the amount of reflection actually felt by the microdisk laser. Comparing the extinction ratios measured on Figs. 10(a) and 10(b) to the ones extracted from the spectral measurements from Figs. 9(a) and 9(b), we demonstrate an 8dB difference in lasing power between the CW and the CCW modes for laser A, and a 6.9dB difference for laser B.

One important requirement for the use of microdisk lasers in optical interconnects is to demonstrate that devices do not lase in different directions or switch from one lasing direction to the other depending on the injection current and the temperature. In [20], the LI curves of a microdisk laser at elevated temperatures remain smooth and unidirectional under pulsed driving conditions, in contrast to the case where continuous wave drive conditions were applied. Most likely this is because when the ambient temperature is changed, it affects both the silicon waveguide and the InP-based microdisk cavity, while the self heating effect in continuous wave mode only heats up the disk cavity. In this study, we investigate the influence of the DBR on the unidirectionality of the laser over a broad range of temperatures. The sample was heated by means of a Peltier element, under continuous drive conditions. The temperature was increased from 10°C to 35°C with the following steps 10°C, 15°C, 20°C, etc. As the DBR structure is designed to be 55 μm away from the microdisk laser, this corresponds to approximately a 2 radian phase change for the reflected light. Figure 11 shows the optical power-current (LI) characteristic of laser B for the different ambient temperatures of the stage. Optical powers coupling out of the grating couplers in the CCW and the CW directions are simultaneously recorded. We demonstrate that due to the presence of the DBR on one side of the waveguide the LI curves remain unidirectional under continuous drive conditions, over a broad range of temperature. Lasing in the CCW direction is measured up to 35°C and a maximum output power of 3 μW is measured in the fiber at 10°C (this corresponds to 15 μW in the silicon waveguide).

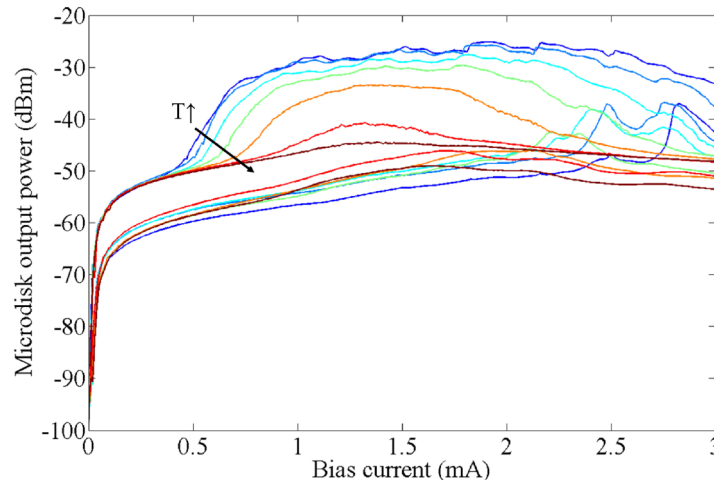


Fig. 11. LI curves of laser B under continuous wave operation at elevated temperatures. The slope efficiency decreases and the threshold current increases at higher temperatures. The power is the fiber coupled output power.

As expected, the threshold current gradually increases with increasing temperature as can be seen in Fig. 11, and the slope efficiency drops. The characteristic temperature of the microdisk laser can be extracted by fitting the natural log of the threshold current versus the ambient temperature. A value of 55K was found, which indicates that the laser is highly sensitive to temperature variations. Some optical power is collected out of the grating coupler above 2.5mA after the DBR in the CW direction of the system. The DBR structure is limited in bandwidth. Heat generated in the microdisk laser leads to a red-shift of its optical spectrum. Because of this red-shift, the longitudinal mode around 1580nm in the CW direction starts to fall out of the bandwidth of the DBR structure. Therefore, optical power is collected in the CW direction for wavelengths outside the bandwidth of the DBR.

5. Conclusion and discussion

In conclusion, we demonstrated and quantified stable unidirectional lasing in microdisk lasers heterogeneously integrated on SOI. Feedback from a passive distributed Bragg reflector is used to achieve stable unidirectional operation. This simple passive design does not add optical losses to the system and does not increase its power consumption. The implementation of this solution is the key to avoid the appearance of a ‘memory’ effect in microdisk lasers. It can be implemented to counteract processing effects, such as sidewall roughness, that threaten unidirectional operation of the lasers. Different devices belonging to the same design can now lase in the same direction with higher efficiency and without switching from one lasing direction to the other depending on the injection current and the temperature. This makes the use of microdisk lasers for optical interconnects applications very attractive.

Acknowledgments

The authors would like to thank the FP7-ICT European Projects HISTORIC and WADIMOS, support from the BOF-Methusalem grant, and the Interuniversity Attraction Poles program of the Belgian Science Policy Office under Grant No. IAP VII/35 “photonics@be”.